Carbohydrate Polymers 88 (2012) 263–269

Contents lists available at SciVerse ScienceDirect

Carbohydrate Polymers

journal homepage: www.elsevier.com/locate/carbpol

Fabrication and antibacterial properties of ZnO–alginate nanocomposites

L.V. Trandafilović[a], D.K. Božanić[a], S. Dimitrijević-Branković[b], A.S. Luyt[c], V. Djoković[a,*]

[a] Vinča Institute of Nuclear Sciences, University of Belgrade, P.O. Box 522, 11001 Belgrade, Serbia
[b] Department of Bioengineering and Biotechnology, Faculty of Technology and Metallurgy, University of Belgrade, Karnegijeva 4, 11120 Belgrade, Serbia
[c] Department of Chemistry, University of the Free State (Qwaqwa Campus), Private Bag X13, Phuthaditjhaba 9866, South Africa

ARTICLE INFO

Article history:
Received 17 August 2011
Received in revised form 17 October 2011
Accepted 1 December 2011
Available online 13 December 2011

Keywords:
Alginate
Nanocomposite
ZnO
Nanoparticles
Antimicrobial activity

ABSTRACT

Alginate was used as a controlled environment for the growth of ZnO nanoparticles. The formation of nanostructured particles was confirmed by a blue shift in the onset of the optical absorption with respect to bulk ZnO. From the XRD measurements it was found that the obtained ZnO nanoparticles have a hexagonal crystal structure. The emission spectrum of the nanocomposite is dominated by a strong band-to-band recombination, while the emission from the ZnO defect states depended on the preparation conditions. Besides showing the presence of Zn 2p, O 1s, Na 1s and C 1s core levels, the XPS analysis also showed that the O 1s spectra can be resolved into two lines that are attributed to the presence of OH groups on the surface of the particles and ZnO, respectively. Antimicrobial tests revealed that the ZnO–alginate nanocomposite exhibits a strong activity against the common pathogens *Staphylococcus aureus* and *Escherichia coli*.

1. Introduction

Nanocomposite materials that comprise inorganic nanoparticles and biopolymers have attracted considerable attention in the last decade (Ruiz-Hitzky, Darder, & Aranda, 2008). Because of the growing interest in eco-friendly and "green" systems, the emphasis of the investigations in the field of nanocomposites was shifted towards biocompatible, renewable and non-toxic matrices. When these features are combined with the size-tunable optical, electronic and catalytic properties of nanoparticles, the possibilities are wide. An important question is can the specific macromolecular structure of biopolymers be used to control the growth and agglomeration of the nanoparticles formed during *in situ* synthesis? Polysaccharides, chitosan (Murugadoss & Chattopadhyay, 2008; Shih, Shieh, & Twu, 2009), starch (Bozanić et al., 2007; Raveendran, Fu, & Wallen, 2003; Vigneshwaran, Kumar, Kathe, Varadarajan, & Prasad, 2006) and alginate (Chang, Yua, Ma, & Anderson, 2011; Gutowska, Jeong, & Jasionowski, 2001) are particularly interesting as matrix polymers since their chains possess large numbers of hydroxyl groups that complex well with metal ions and make them a good environment for the growth of metal and semiconductor nanoparticles.

Alginic acid (alginate) belongs to a family of linear unbranched copolymers of (1,4)-linked β-D-mannuronic (M) and α-L-guluronic (G) acids arranged in a non-regular order along the chain (Chanda, Hirst, Percival, & Ross, 1952). The ratio of M and G acids and their macromolecular conformation determine the physical properties of alginate, its biocompatibility (Orive, Ponce, Hernández, Gascón, Igartua, & Pedraz, 2002) and biodegradability under normal physiological conditions (Becker, Kipke, & Brandon, 2001), as well as its reactions with metal ions (Smidsrød & Haug, 1965a,b). Alginate is widely used as an instant gel for bone tissue engineering (Gutowska et al., 2001), drug delivery (Bouhadir, Alsberg, & Mooney, 2001), protein immobilization (Volodkin, Larionova, & Sukhorukov, 2004) etc. Alginate also exhibits affinity towards divalent metal ions that have been used for the stabilization of inorganic nanoparticles (Brayner, Vaulay, Fiévet, & Coradin, 2007; Ma, Qi, Maitani, & Nagai, 2007). Recently Ma et al. (2007) applied alginate stabilized iron oxide nanoparticles for detecting liver cancer. In the present study we used the alginate in order to achieve controlled synthesis of ZnO nanoparticles and investigate their structural, optical and antimicrobial properties.

ZnO is a transition metal oxide with good catalytic, electrical, photochemical and optical properties (Ashour, Kaid, Elsayed, & Ibrahim, 2006; Brida et al., 2002; Wang, 2004). It has a wide band gap (E_g = 3.37 eV), large exciton binding energy (60 meV) (Tan et al., 2005), and finds application as a material for gas sensors, solar cells, display screens, photocell electrodes, and UV-light emitting diodes (Dong, Cui, & Zhang, 1997; Ginley & Bright, 2000; Haraa et al., 2000; Keis, Vayssieres, Lindquist, & Hagfeldt, 1999). In the area of bioscience it was shown that nano ZnO can be useful as a biomimic membrane; it can immobilize and modify proteins because of the fast electron transfer between the enzyme's active sites and the electrode (Corso, Dickherber, & Hunt,

* Corresponding author. Tel.: +381 118066428; fax: +381 113440100.
E-mail address: djokovic@vinca.rs (V. Djoković).

0144-8617/$ – see front matter © 2011 Elsevier Ltd. All rights reserved.
doi:10.1016/j.carbpol.2011.12.005

2007; Dorfman, Kumar, & Hahm, 2006a,b; Krishnamoorthy, Bei, Zoumakis, Chrousos, & Iliadis, 2006; Wang et al., 2006; Wei et al., 2006; Zhu, Yuri, Gan, Suzuki, & Li, 2007). As antibacterial agent ZnO has several advantages: noticeable activity in the pH neutral region (pH = 7–8) without the presence of light (Applerot et al., 2009; Jones, Ray, Ranjit, & Manna, 2008; Sawai et al., 1996; Yamamoto, 2001; Yamamoto, Nakakoshi, Sasamoto, Nakagawa, & Miura, 2001). The particular mechanism of the antimicrobial activity of ZnO is still a matter of dispute. Some researchers consider that it might be a consequence of the generation of hydrogen peroxide (H_2O_2) on its surface (Applerot et al., 2009; Jalal et al., 2010; Jones et al., 2008; Sawai, 2003; Sawai et al., 1996, 1998; Stoimenov, Klinger, Marchin, & Klabunde, 2002; Sunada, Kikuchi, Hashimoto, & Fujishima, 1998; Yamamoto et al., 2001).

In a recent study, Baskoutas et al. (2007) prepared ZnO nanoparticles by thermal decomposition of zinc–alginate at high temperatures (800 °C). Here we used a different approach by synthesizing ZnO nanoparticles within alginate using microwave radiation. The nanoparticles formed in the presence of alginate were characterized by optical and structural methods. On the other hand, it has already been shown that the biocompatibility of polysaccharide based nanocomposites is an advantage in the medical application of these materials, while the starch–ZnO nanocomposites can be successfully used in the preparation of cotton fabrics with antimicrobial properties (Vigneshwaran et al., 2006). For this reason we considered that it could be interesting from a practical point of view to investigate the antimicrobial activity of the obtained ZnO–alginate nanocomposites. In the second part of the study the antimicrobial activity of the nanocomposite solutions was tested versus the common pathogens *Staphylococcus aureus* and *Escherichia coli*.

2. Experimental

2.1. Preparation of ZnO–alginate nanocomposites

Alginate from brown algae with $M_r \sim 48{,}000$–$186{,}000$ (Biochemica) Fluka was used in the present study. Zinc acetate and sodium hydroxide were purchased from Merck and used as received. A micron size zinc oxide powder (particle size ~ 1 μm) was obtained from Sigma Aldrich. The alginate solution was prepared by dissolving 1 g of alginate in 100 mL of 0.01 M NaOH solution. In a typical synthetic procedure for the preparation of ZnO–alginate nanocomposites, 0.8 mL of 1 M NaOH solution was first added to 2 mL of 0.2 M Zn-acetate water solution. To that mixture, 5 mL of 1% sodium alginate solution was added drop by drop. The obtained mixtures were then placed in the microwave (MW) oven and treated at 800 W for various times (30 s, 1 min and 5 min). The solid alginate–ZnO nanocomposite was collected with slow centrifugation, washed several times with deionized water and dried in a vacuum oven at 40 °C. The samples obtained after 30 s, 1 min and 5 min of MW treatment are further in the text denoted as a-ZnO-1, a-ZnO-2 and a-ZnO-3, respectively. The amount of zinc oxide in the nanocomposites was determined by atomic absorption spectroscopy and found to be ~11 wt.%.

2.2. Methods

The X-ray diffraction (XRD) measurements were performed on a Philips PW1050 X-ray diffractometer (Cu-K_α source, $\lambda = 0.154$ nm). Transmission electron microscopy (TEM) measurements were carried out by using a Phillips CM100 instruments with operating voltage 100 keV. The samples were prepared by placing a drop of the ZnO–alginate nanocomposite water solution onto a carbon-coated copper grid. UV–vis absorption spectra of a water solution of the nanocomposites and a water dispersion of the ZnO micropowder were obtained by using a Perkin Elmer Lambda 5 UV-VIS spectrophotometer. The luminescence spectra were recorded on the same samples at 320 nm excitation wavelength on a Perkin Elmer LS 3B spectrophotometer. X-ray photoelectron spectroscopy (XPS) experiments were performed on a Physical Electronics Quantum 2000 instrument using Al K_α radiation (1486.6 eV). The peak shift due to charge accumulation was corrected using the C 1s level at 284.4 eV as an internal standard (Powell, 1995). The XPS peaks are assumed to be linear combinations of Lorentzian and Gaussian line shapes and were resolved into individual components after proper subtraction of the baseline using the Shirley background subtraction method. The atomic absorption analysis was carried on a Varian AA-1475 spectrophotometer.

2.3. Microorganisms and culture conditions

Microorganisms used in this study are Gram-negative bacteria *E. coli* ATCC 25923 and Gram-positive bacteria *S. aureus* ATCC 25922. The inoculum of the microorganism was prepared in a trypton soy broth (Torlak, Serbia) with 0.6% yeast extract (TSBY), which was used as a growing medium. The microorganisms were cultivated in 3 mL TSBY at 37 °C and left overnight (late exponential stage of growth). A potassium hydrogen phosphate buffer solution (pH 7.2) was used as a medium for quantitative testing of the microbicidal activity of the samples. Pure agar solution was used as the control sample.

2.4. Antimicrobial activity testing

The quantitative testing of alginate–ZnO nanocomposite antimicrobial activity was assessed according to the ASTM E 2149-01 standard. The alginate–ZnO samples were prepared by dissolving 15 mg of solid nanocomposite in 15 mL of water. The control sample as well as 0.1 and 1 mL of each of the nanocomposite solutions were added into glass tubes containing 9 mL of buffer solution inoculated with 1 mL of diluted microbial inoculum (so that the initial numbers of *S. aureus* and *E. coli* in inoculums were $\sim 10^5$ CFU/mL). The test tube was further put in a water bath shaker and the solution was incubated at 37 °C. After 1 and 2 h of exposure, 0.1 mL aliquots were removed and further diluted with sterile physiological saline solution (8.5 g NaCl in 1 L of water). From all dilutions 0.1 mL aliquots were placed in Petri dishes, over layered with trypton soy agar and after 24 h incubation at 37 °C, the number of viable bacteria was counted. The percentage of bacteria reduction (R, %) was calculated as:

$$R = \frac{C_0 - C}{C_0}, \quad (1)$$

where C_0 (in CFU) is the number of bacterial colonies from the control saline and C (in CFU) is the number of bacterial colonies from the samples.

3. Results and discussion

3.1. Morphology and structure

The formation of the ZnO nanoparticles in the presence of alginate possibly occurs according to following chemical reactions (Zhang & Mu, 2007):

$$Zn^{2+} + 4OH^- \rightarrow Zn(OH)_4^{2-} \quad (R1)$$

and

$$Zn(OH)_4^{2-} \rightarrow ZnO + 2H_2O + 2OH^- \quad (R2)$$

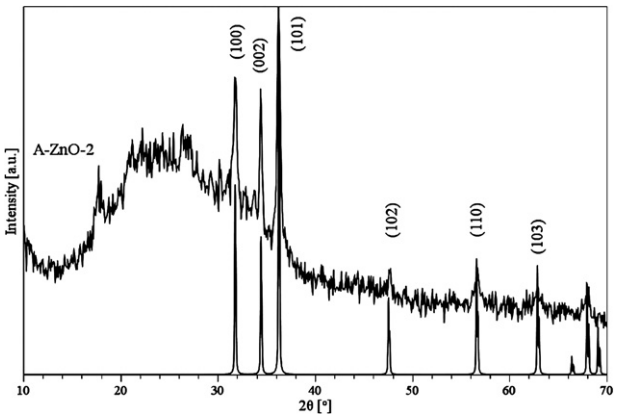

Fig. 1. XRD spectrum of the a-ZnO-2 nanocomposite film.

In the first reaction the Zn^{2+} ions react with OH^- creating the precursor $Zn(OH)_4^{2-}$, which upon heating bond together forming the cluster $[Zn_xO_y(OH)_z]^{(z+2\,y-2x)-}$ (Li, Shi, Zhong, & Yin, 1999). During the ZnO crystal growth, this cluster is incorporated into the lattice. On the other hand, alginate poly G-sequences tend to adopt an ordered confirmation through dimerization in the presence of divalent metals (Morris, Rees, Thom, & Boyd, 1978; Brayner et al., 2007), so they act as a controlled environment for the growth of particles of nanometer sizes.

The a-ZnO-2 sample was chosen to illustrate the crystal structure of the ZnO nanoparticles in the alginate matrix. The results of the XRD analysis of the a-ZnO-1 and a-ZnO-3 samples were similar to that of a-ZnO-2 and for this reason they will not be reported. The XRD spectrum of a-ZnO-2 nanocomposite film is shown in Fig. 1. The broad diffraction peak positioned at low angles originates from the alginate matrix while the other peaks correspond to the (1 0 0), (0 0 2), (1 0 1), (1 0 2), (1 1 0) and (1 0 3) planes of hexagonal bulk ZnO (Sawada, Wang, & Sleigh, 1996). The transmission electron microscopy (TEM) images of the a-ZnO-1, a-ZnO-2 and a-ZnO-3 samples are presented in Figs. 2a, 3a and 4a. The micrographs depict a large number of spherical particles well dispersed in the alginate matrix. The corresponding electron diffraction pattern (inset in Fig. 3a) shows that the obtained ZnO nanoparticles are polycrystalline. The size distributions of the nanoparticles (Figs. 2b, 3b and 4b) obtained from the TEM images are relatively narrow with average sizes D_{LN} = 6.8 nm, 3.9 nm and 4.7, respectively. This proves that the alginate can efficiently control the growth of the ZnO nanoparticles although the width of the size distribution depended on the time of treatment (the estimated polydispersities for a-ZnO-1, a-ZnO-2 and a-ZnO-3 samples were found to be 63, 55 and 34%, respectively). It should be noted that the average size of the nanoparticles in a-ZnO-2 sample obtained from the half-width of the (0 0 2) diffraction peak using Scherrer's equation was found to be 16.7 nm, which is higher than the 3.8 nm obtained from the TEM measurements. However, the small number of bigger particles (Fig. 3b) actually represents a larger portion of the total mass of the sample and they will contribute more to the XRD signal, which consequently leads to the observed discrepancy between the estimated sizes obtained by TEM and XRD analyses.

3.2. Optical properties

The UV–vis absorption curves of the a-ZnO-1, a-ZnO-2 and a-ZnO-3 nanocomposites are presented in Fig. 5a. In the inset of the same figure, the UV–vis absorption of the water dispersion of the ZnO micro-powder is shown. As can be seen, the positions of the absorption peaks (Fig. 5a) were shifted towards lower wavelengths

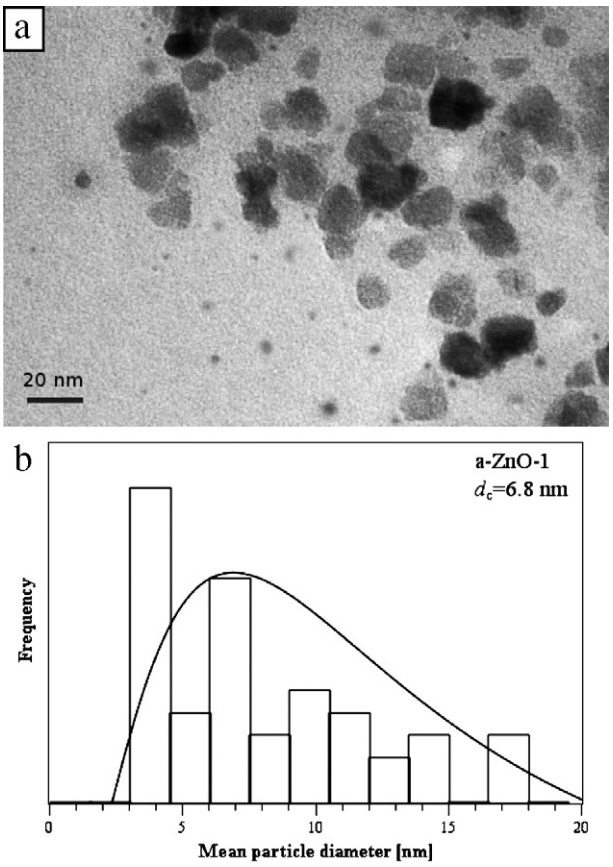

Fig. 2. (a) TEM micrograph of the a-ZnO-1 nanocomposite sample and ED pattern of the ZnO nanoparticles. (b) Size distribution of the nanoparticles (93 particles were counted for the histogram). The histograms were fitted by a log-normal distribution curve with parameters D_{LN} = 6.8 nm, σ_{LN} = 1.5.

with respect to the absorption of bulk ZnO (380 nm, inset) indicating the presence of nano-size particles. The strongest shift of 20 nm was observed for the a-ZnO-3 sample. According to calculations based on the effective mass model (Pesika, Stebe, & Searson, 2003), the obtained shift corresponds to an average particle size of 3.2 nm, which is close to the average size of 4.7 nm obtained from TEM analysis (Fig. 4b). The fluorescence spectra of the three nanocomposite films obtained after excitation at 320 nm are shown in Fig. 5b. The spectra show a dominant peak at around 385 nm (3.22 eV) attributed to the radiative exciton annihilation. This peak can be found in the PL spectrum of undoped high-quality ZnO (Özgür et al., 2005; Thonke et al., 2001) and in the spectra of ZnO micron-powder is positioned at ~390 nm (Fig. 5b, inset). The peaks positioned at wavelengths higher than 390 nm (Fig. 3b) originate from different defects in the crystal structure of ZnO such as oxygen vacancies, antisites or impurities. For instance, the peak around 421 nm is attributed to the recombination of an electron at the zinc interstitial (Zn_i) and a hole in the valence band (Vanheusden, Seager, Warren, Tallant, & Voigt, 1996). The emission peak at 446 nm originates from the electron transition of a shallow oxygen vacancy and zinc interstitial levels to the valence band (Zhang, Xue, & Wang, 2002). The emissions at 460 and 485 nm come from the single ionized oxygen vacancies (Zhang, Wang, & Xue, 2003). Some authors attribute the luminescence peak at 485 nm to a surface state transition which is present solely in the quantum dots but not in the bulk ZnO (Borgohain & Mahamuni, 1998). The emission in the green region (~530 nm) is usually present in the bulk as well as in the nanostructured ZnO. The green luminescence is also attributed to defect levels arising from the presence of the oxygen vacancies and/or

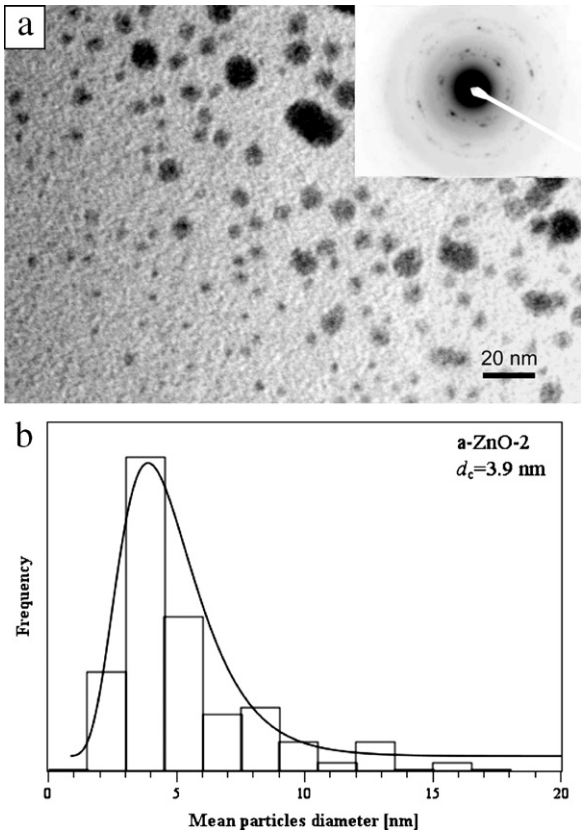

Fig. 3. (a) TEM micrograph of the a-ZnO-2 nanocomposite sample and (inset) ED pattern of the ZnO nanoparticles. (b) Size distribution of the nanoparticles (124 particles were counted for the histogram). The histograms were fitted by a log-normal distribution curve with parameters D_{LN} = 3.9 nm, σ_{LN} = 0.8.

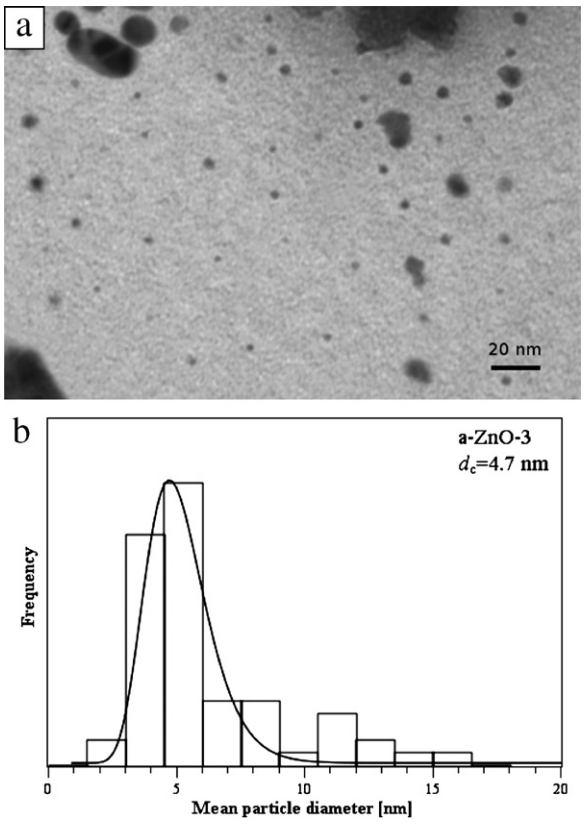

Fig. 4. (a) TEM micrograph of the a-ZnO-3 nanocomposite sample. (b) Size distribution of the nanoparticles (88 particles were counted for the histogram). The histograms were fitted by a log-normal distribution curve with parameters D_{LN} = 4.7 nm, σ_{LN} = 0.5.

the zinc interstitials (Kamat & Patrick, 1992; Spanhel & Anderson, 1991). A comparison of the photoluminescence spectra in Fig. 5b also suggests that prolonged treatment induces an increase in the number of defects in the ZnO nanoparticles.

3.3. XPS spectra

The catalytic properties and antimicrobial activity strongly depend on the structure and stability of the different surface planes of ZnO as well as the number of defects on the ZnO particle surfaces (Joshi, Sahai, Gandhi, Krishna, & Haranath, 2010; Kotsis & Staemmler, 2006; Padmavathy & Vijayaraghavan, 2008; Sunada et al., 1998). For this reason we used X-ray photoelectron spectroscopy, a technique highly sensitive to the chemical composition and the environments of the elements in the material, to study the ZnO nanoparticles in the alginate matrix. According to Kotsis and Staemmler (2006), the XPS O1s peak positions depend quite sensitively on the oxidation state and chemical environment of the O atom under consideration, and enable one to easy distinguish O atoms in the bulk ZnO from those on the surface. An initial XPS survey scan of the a-ZnO-2 nanocomposite film shows the presence of Zn 2p, O 1s, Na 1s and C 1s core levels. The high resolution spectra of the Zn 2p and O 1s levels are shown in Fig. 6. In the high-resolution spectra of the Zn 2p level (Fig. 6a) two distinct lines at 1021.4 eV and 1044.5 eV can be noticed, that are the consequence of spin orbital splitting and correspond to the Zn $2p_{3/2}$ and Zn $2p_{1/2}$ core levels. Fig. 6b shows the O 1s spectrum that could be resolved in two peaks positioned at 530.9 and 535.5 eV. The low-binding-energy component at 530.9 eV is assigned to the O atoms from the bulk ZnO (Kotsis & Staemmler, 2006). The line at 535.53 eV is attributed to the presence of OH groups on the ZnO surface (Joshi et al., 2010; Kotsis & Staemmler, 2006).

3.4. Antimicrobial activity

The antimicrobial activity tests were carried out against the bacteria *S. aureus* and *E. coli*. The advantage of fabrication of the ZnO nanoparticles in the presence of alginate is that it can play the

Table 1
Results of antimicrobial activity testing of a-ZnO nanocomposites (0.1 mL of the nanocomposite solutions were tested).

	Staphylococcus aureus				*Escherichia coli*			
	1 h		2 h		1 h		2 h	
	CFU	*R* [%]	CFU	*R* [%]	CFU	*R* [%]	CFU	*R* [%]
Control	3.1×10^5	–	4.9×10^5	–	4.5×10^5	–	1.6×10^6	–
a-ZnO-1	3.0×10^3	99.03	5.4×10^2	99.88	4.0×10^2	99.91	–	100
a-ZnO-2	2.8×10^3	99.09	6.4×10^2	99.87	2.2×10^2	99.95	2.0×10^1	99.99
a-ZnO-3	5.7×10^2	99.81	4.2×10^2	99.91	5.0×10^1	99.98	–	100

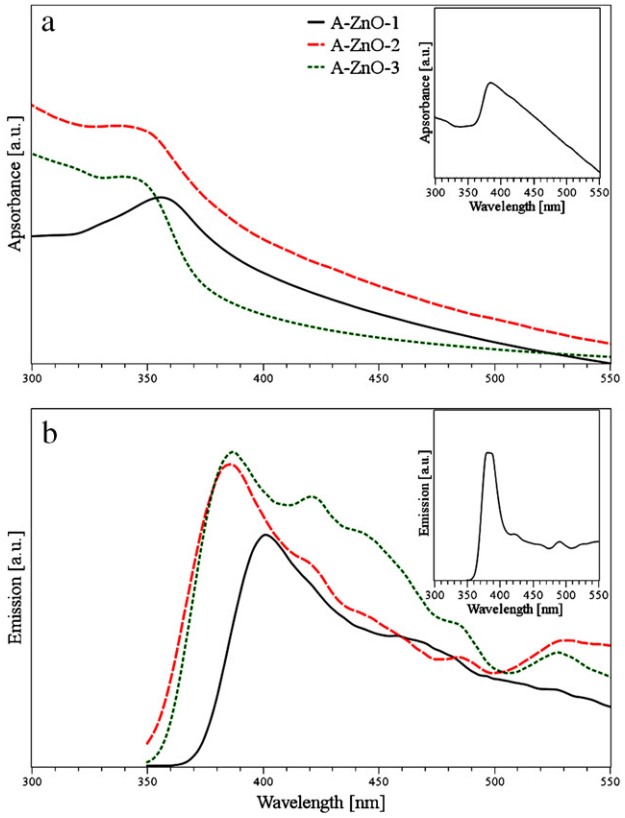

Fig. 5. (a) UV–vis absorption spectra and (b) photoluminescence spectra of a-ZnO-1, a-ZnO-2 and a-ZnO-3 nanocomposites. The insets show the absorption and PL spectra of the micron size ZnO powder.

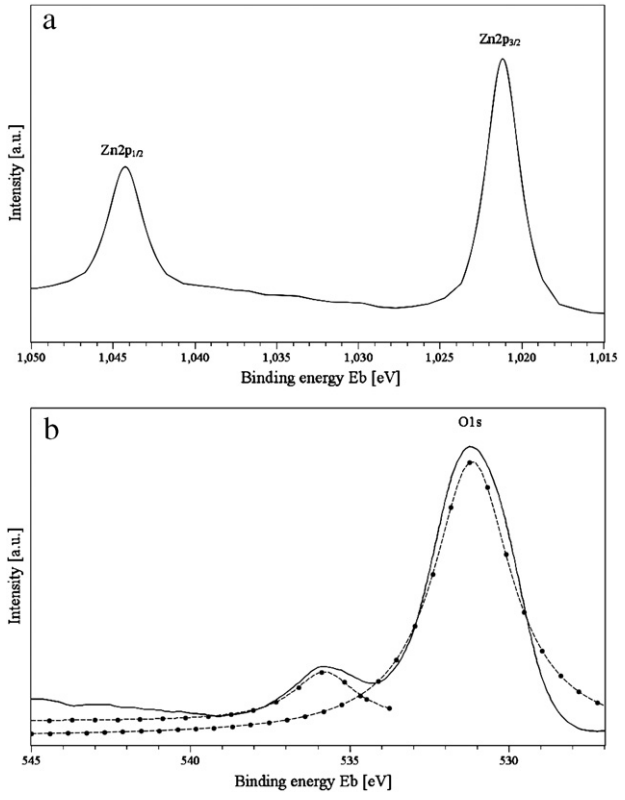

Fig. 6. XPS spectra of the a-ZnO-2 nanocomposite film: (a) Zn 2p and (b) O 1s core levels.

role of a stabilization agent as well as the role of the matrix of the solid nanocomposite. Both types of samples (nanocomposite solutions and thin films) showed strong antimicrobial activity but we decided to test the activity of the samples in solution. Table 1 shows the results obtained for the control sample and 0.1 mL solutions of three nanocomposites. It can be seen in Table 1 that after 1 h of exposure the a-ZnO-1, a-ZnO-2 and a-ZnO-3 nanocomposites showed strong bactericidal activity, with the lowest efficiency of about 99.03% of reduction observed for a-ZnO-1. After 2 h, the reduction was over 99.9% for *S. aureus* and 100% for *E. coli*. The bactericidal effects of nano ZnO have been explained by the production of highly reactive oxygen species (ROS) (OH^-, H_2O_2 and O_2^{2-}) on the surface of the nanoparticles connected with fatal damage to the bacteria (Applerot et al., 2009; Sawai et al., 1996; Stoimenov et al., 2002). However, some other studies suggest that the formation of H_2O_2 is the primary effect that contributes to the antibacterial activity, which takes place *via* penetration of H_2O_2 through the cell walls (Jalal et al., 2010; Sawai et al., 1998). The generation of H_2O_2 depends strongly on the specific surface area of ZnO, which results in more oxygen species, more hydrogen peroxide and higher antibacterial activity of the smaller nanoparticles (Padmavathy & Vijayaraghavan, 2008; Sunada et al., 1998). Another possible explanation for the antibacterial effect is based on the abrasive surface texture of ZnO due to surface defects (Padmavathy & Vijayaraghavan, 2008; Stoimenov et al., 2002). The abrasiveness of ZnO nanoparticles compared to bulk ZnO is caused by the uneven surface texture due to rough edges and corners that contribute to the mechanical damage to the cell membrane of the bacteria.

It should be noted that we chose the amount of the nanocomposite solution to be 0.1 mL in order to investigate whether the preparation of the samples can affect the antimicrobial activity and establish if there is a difference in their action towards Gram-negative and Gram-positive bacteria. The higher amount (1 mL) of all three nanocomposite samples, with ten times higher concentration of ZnO, killed all the bacteria after 1 h and we could not derive any conclusion from the obtained results. For this reason only the results obtained for 0.1 mL of the nanocomposite solution are reported in Table 1. By changing the time of microwave treatment during the preparation of the ZnO nanoparticles in the presence of the alginate, we tried to induce more surface defects (which is followed up via emission spectra in Fig. 5b). The sample prepared with the longest MW treatment (5 min) showed slightly better activity after 1 h of exposure while the results after 2 h are comparable for all the samples. Assuming that an increase in the number of surface defects (due to higher catalytic activity) facilitates the peroxide formation might possibly explain the improved activity of the a-ZnO-3 sample at shorter exposure times. The results in Table 1 also show that *S. aureus* is slightly more resistant then *E. coli* to the action of ZnO nanoparticles especially at lower time of exposure (1 h), which is in agreement with previously published reports (Applerot et al., 2009; Yamamoto, 2001; Yamamoto et al., 2001). Several factors can explain the different results of the antibacterial tests for *S. aureus* and *E. coli*. The cell wall attributes differ between Gram-negative and Gram-positive bacteria (Heijenoort, 2001). *E. coli* (Gram negative bacteria) has a relatively thin cell wall made of peptidoglycans and lipopolysaccharide. On the other hand, *S. aureus* (Gram-positive bacteria) has a thick cell wall, consisting of a large amount of mucopeptides, murein and lipoteichoic acids (immunostimulator molecule). Also, the golden carotenoid pigments and the antioxidant enzymes (catalase) of *S. aureus* give this bacteria a bit stronger oxidant resistance (Liu et al., 2005; Makhluf et al., 2005; Schwartz et al., 1983). Besides cell-wall properties, some other factors such as cell permeability, capability of solubilizing ZnO and extracting harmful Zn^{2+} ions might also be considered (Fasim, Ahmed, Parsons, & Gadd, 2002).

4. Conclusion

ZnO nanoparticles were prepared within an alginate biopolymer by microwave treatment. The obtained nanoparticles were mostly spherical in shape and had a hexagonal crystal structure. The onset of the absorption of the ZnO–alginate nanocomposite solutions was shifted towards a lower wavelength due to the nano-size dimensions of the particles. A band to band recombination dominates the PL spectra of all the samples, while the intensity of the peaks that originate from the defects on the nanoparticle surfaces increase with time of MW treatment. Antibacterial activity tests were carried out with *S. aureus* and *E. coli* pathogens. All the ZnO–alginate nanocomposite samples showed fast and strong antibacterial activity, with 99.9% reduction for *S. aureus* and 100% reduction for *E. coli* after 2 h of exposure.

Acknowledgement

This work was supported in part by the Ministry of Education and Science, Republic of Serbia (Project Nos. 172056 and 45020).

References

Applerot, G., Lipovsky, A., Dror, R., Perkas, N., Nitzan, Y., Lubart, R., et al. (2009). Enhanced antibacterial activity of nanocrystalline ZnO due to increased ros-mediated cell injury. *Advanced Functional Materials*, *19*, 842–852.

Ashour, A., Kaid, M., Elsayed, N., & Ibrahim, A. (2006). Physical properties of ZnO thin films deposited by spray pyrolysis technique. *Applied Surface Science*, *252*, 7844–7848.

Baskoutas, S., Giabouranis, P., Yannopoulos, S., Dracopoulos, V., Toth, L., Chrissanthopoulos, A., et al. (2007). Preparation of ZnO nanoparticles by thermal decomposition of zinc alginate. *Thin Solid Films*, *515*, 8461–8464.

Becker, T. A., Kipke, D. R., & Brandon, T. (2001). Calcium alginate gel: A biocompatible and mechanically stable polymer for endovascular embolization. *Journal of Biomedical Materials Research*, *54*, 76–86.

Borgohain, K., & Mahamuni, S. (1998). Luminescence behaviour of chemically grown ZnO quantum dots. *Semiconductor Science and Technology*, *13*, 1154.

Bouhadir, K., Alsberg, E., & Mooney, D. (2001). Hydrogels for combination delivery of antineoplastic agents. *Biomaterials*, *22*, 2625–2633.

Bozanić, D., Djoković, V., Blanuša, J., Nair, P. S., Georges, M., & Radhakrishnan, T. (2007). Preparation and properties of nano-sized Ag and Ag_2S particles in biopolymer matrix. *The European Physical Journal E*, *22*, 51–59.

Brayner, R., Vaulay, M.-J., Fiévet, F., & Coradin, T. (2007). Alginate-mediated growth of Co, Ni, and CoNi nanoparticles: Influence of the biopolymer structure. *Chemistry of Materials*, *19*, 1190–1198.

Brida, D., Fortunato, E., Águas, H., Silva, V., Marques, A., Pereira, L., et al. (2002). New insights on large area flexible position sensitive detectors. *Journal of Non-Crystalline Solids*, *299-302*, 1272–1276.

Chanda, S. K., Hirst, L., Percival, E. G. V., & Ross, A. G. (1952). The structure of alginic acid. Part II. *Journal of the Chemical Society*, 1837–1933.

Chang, P. R., Yua, J., Ma, X., & Anderson, D. P. (2011). Polysaccharides as stabilizers for the synthesis of magnetic nanoparticles. *Carbohydrate Polymers*, *83*, 640–644.

Corso, C. D., Dickherber, A., & Hunt, W. D. (2007). Lateral field excitation of thickness shear mode waves in a thin film ZnO solidly mounted resonator. *Journal of Applied Physics*, *89*, 1–8.

Dong, L., Cui, Z. L., & Zhang, Z. K. (1997). Gas sensing properties of nano-ZnO prepared by arc plasma method. *Nanostructured Materials*, *8*, 815–823.

Dorfman, A., Kumar, N., & Hahm, J. (2006a). Nanoscale ZnO-enhanced fluorescence detection of protein interactions. *Advanced Materials*, *18*, 2685–2690.

Dorfman, A., Kumar, N., & Hahm, J. (2006b). Highly sensitive biomolecular fluorescence detection using nanoscale ZnO platforms. *Langmuir*, *22*, 4890–4895.

Fasim, F., Ahmed, N., Parsons, R., & Gadd, G. M. (2002). Solubilization of zinc salts by a bacterium isolated from the air environment of a tannery. *FEMS Microbiology Letters*, *213*, 1–6.

Ginley, D., & Bright, C. (2000). Transparent conducting oxides. *MRS Bulletin*, *25*, 15–18.

Gutowska, A., Jeong, B., & Jasionowski, M. (2001). Injectable gels for tissue engineering. *The Anatomical Record*, *263*, 342–3499.

Haraa, K., Horiguchib, T., Kinoshitab, T., Sayamaa, K., Sugiharaa, H., & Arakawaa, H. (2000). Highly efficient photon-to-electron conversion with mercurochrome-sensitized nanoporous oxide semiconductor solar cells. *Solar Energy Materials and Solar Cells*, *64*, 115–134.

Heijenoort, J. (2001). Formation of the glycan chains in the synthesis of bacterial peptidoglycan. *Glycobiology*, *11*, 25R–36R.

Jalal, R., Goharshadi, E. K., Abareshi, M., Moosavi, M., Yousefi, A., & Nancarrow, P. (2010). ZnO nanofluids: Green synthesis, characterization, and antibacterial activity. *Materials Chemistry and Physics*, *121*, 198–201.

Jones, N., Ray, B., Ranjit, K. T., & Manna, A. C. (2008). Antibacterial activity of ZnO nanoparticle suspensions on a broad spectrum of microorganisms. *FEMS Microbiology Letters*, *279*, 71–76.

Joshi, A. G., Sahai, S., Gandhi, N., Krishna, Y. G. R., & Haranath, D. (2010). Valence band and core-level analysis of highly luminescent ZnO nanocrystals for designing ultrafast optical sensors. *Applied Physics Letters*, *96*, 123102–123105.

Kamat, P. V., & Patrick, B. (1992). Photophysics and photochemistry of quantized zinc oxide colloids. *Journal of Physical Chemistry*, *96*, 6829–6834.

Keis, K., Vayssieres, L., Lindquist, S., & Hagfeldt, A. (1999). Nanostructured ZnO electrodes for photovoltaic applications. *Nanostructured Materials*, *12*, 487–490.

Kotsis, K., & Staemmler, V. (2006). Ab initio calculations of the O1s XPS spectra of ZnO and Zn oxo compounds. *Physical Chemistry Chemical Physics*, *8*, 1490–1498.

Krishnamoorthy, S., Bei, T., Zoumakis, E., Chrousos, G. P., & Iliadis, A. A. (2006). Morphological and binding properties of interleukin-6 on thin ZnO films grown on (1 0 0) silicon substrates for biosensor applications. *Biosensors and Bioelectronics*, *22*, 707–714.

Li, W. J., Shi, E. W., Zhong, W. Z., & Yin, Z. W. (1999). Growth mechanism and growth habit of oxide crystals. *Journal of Crystal Growth*, *203*, 186–196.

Liu, G., Essex, A., Buchanan, J., Datta, V., Hoffman, H., Bastian, J., et al. (2005). *Staphylococcus aureus* golden pigment impairs neutrophil killing and promotes virulence through its antioxidant activity. *Journal of Experimental Medicine*, *202*, 209–215.

Ma, H.-L., Qi, X.-R., Maitani, Y., & Nagai, T. (2007). Preparation and characterization of superparamagnetic iron oxide nanoparticles stabilized by alginate. *International Journal of Pharmaceutics*, *333*, 177–186.

Makhluf, S., Dror, R., Nitzan, Y., Abramovich, Y., Jelinek, R., & Gedanken, A. (2005). Microwave-assisted synthesis of nanocrystalline MgO and its use as a bacteriocide. *Advanced Functional Materials*, *15*, 1708–1715.

Morris, E. R., Rees, D. A., Thom, D., & Boyd, J. (1978). Chiroptical and stoichiometric evidence of a specific, primary dimerization process in alginate gelation. *Carbohydryte Research*, *66*, 145–154.

Murugadoss, A., & Chattopadhyay, A. (2008). A 'green' chitosan–silver nanoparticle composite as a heterogeneous as well as micro-heterogeneous catalyst. *Nanotechnology*, *19*, 015603.

Orive, G., Ponce, S., Hernández, R. M., Gascón, A. R., Igartua, M., & Pedraz, J. L. (2002). Biocompatibility of microcapsules for cell immobilization elaborated with different type of alginates. *Biomaterials*, *23*, 3825–3831.

Özgür, Ü., Alivov, Y. I., Liu, C., Teke, A., Reshchikov, M. A., Doğan, S., et al. (2005). A comprehensive review of ZnO materials and devices. *Journal of Applied Physics*, *98*, 041301.

Padmavathy, N., & Vijayaraghavan, R. (2008). Enhanced bioactivity of ZnO nanoparticles: An antimicrobial study. *Science and Technology of Advanced Materials*, *9*, 035004.

Pesika, N. S., Stebe, K. J., & Searson, P. C. (2003). Relationship between absorbance spectra and particle size distributions for quantum-sized nanocrystals. *Journal of Physical Chemistry B*, *107*, 10412–10415.

Powell, C. (1995). Referenca za korekciju XPSa. *Applied Surface Science*, *89*, 141–149.

Raveendran, P., Fu, J., & Wallen, S. L. (2003). Completely green synthesis and stabilization of metal nanoparticles. *Journal of the American Chemical Society*, *125*, 13940–13941.

Ruiz-Hitzky, E., Darder, M., & Aranda, P. (2008). An introduction to bio-nanohybrid materials. In E. Ruiz-Hitzky, K. Ariga, & Y. M. Lvov (Eds.), *Bio-inorganic hybrid nanomaterials*. Wiley-VCH Verlag.

Sawada, H., Wang, R., & Sleigh, A. (1996). An electron density residual study of zinc oxide. *Journal of Solid State Chemistry*, *122*, 148–150.

Sawai, J. (2003). Quantitative evaluation of antibacterial activities of metallic oxide powders (ZnO, MgO and CaO) by conductimetric assay. *Journal of Microbiological Methods*, *54*, 177–182.

Sawai, J., Kawada, E., Kanou, F., Igarashi, H., Hashimoto, A., Kokugan, T., et al. (1996). Detection of active oxygen generated from ceramic powders having antibacterial activity. *Journal of Chemical Engineering of Japan*, *29*, 627–633.

Sawai, J., Shoji, S., Igarashi, H., Hashimoto, A., Kokugan, T., Shimizu, M., et al. (1998). Hydrogen peroxide as an antibacterial factor in zinc oxide powder slurry. *Journal of Fermentation and Bioengineering*, *86*, 521–522.

Schwartz, C. E., Krall, J., Norton, L., McKay, K., Kay, D., & Lynch, R. E. (1983). Catalase and superoxide dismutase in *Escherichia coli*. *Journal of Biological Chemistry*, *258*, 6277–6281.

Shih, C.-M., Shieh, Y.-T., & Twu, Y.-K. (2009). Preparation of gold nanopowders and nanoparticles using chitosan suspensions. *Carbohydrate Polymers*, *78*, 309–315.

Smidsrød, O., & Haug, A. (1965a). The effect of divalent metals on the properties of alginate solutions. I. Calcium ions. *Acta Chemica Scandinavica*, *19*, 329–340.

Smidsrød, O., & Haug, A. (1965b). The effect of divalent metals on the properties of alginate solutions. II. Comparison of different metal ions. *Acta Chemica Scandinavica*, *19*, 341–351.

Spanhel, L., & Anderson, M. A. (1991). Semiconductor clusters in the sol–gel process: Quantized aggregation, gelation, and crystal growth in concentrated zinc oxide colloids. *Journal of the American Chemical Society*, *113*, 2826–2833.

Stoimenov, P. K., Klinger, R. L., Marchin, G. L., & Klabunde, K. J. (2002). Metal oxide nanoparticles as bactericidal agents. *Langmuir*, *18*, 6679–6686.

Sunada, K., Kikuchi, Y., Hashimoto, K., & Fujishima, A. (1998). Bactericidal and detoxification effects of TiO_2 thin film photocatalysts. *Environmental Science and Technology*, *32*, 726–728.

Tan, S. T., Chen, B. J., Sun, X. W., Fan, W. J., Kwok, H. S., Zhang, X. H., et al. (2005). Blueshift of optical band gap in ZnO thin films grown by metal–organic chemical-vapor deposition. *Journal of Applied Physics*, *98*, 013505–13511.

Thonke, K., Gruber, T., Teofilov, N., Schönfelder, R., Waag, A., & Sauer, R. (2001). Donor–acceptor pair transitions in ZnO substrate material. *Physica B: Condensed Matter*, *308–310*, 945–948.

Vanheusden, K., Seager, C. H., Warren, W. L., Tallant, D. R., & Voigt, J. A. (1996). Correlation between photoluminescence and oxygen vacancies in ZnO phosphors. *Applied Physics Letters*, *68*, 403–405.

Vigneshwaran, N., Kumar, S., Kathe, A. A., Varadarajan, P. V., & Prasad, V. (2006). Functional finishing of cotton fabrics using zinc oxide–soluble starch nanocomposites. *Nanotechnology*, *17*, 5087–5095.

Volodkin, D. V., Larionova, N. I., & Sukhorukov, G. B. (2004). Protein encapsulation via porous $CaCO_3$ microparticles templating. *Biomacromolecules*, *5*, 1962–1972.

Wang, Z., Yang, Y., Li, J., Gong, J., Shen, G., & Yu, R. (2006). Organic–inorganic matrix for electrochemical immunoassay: Detection of human IgG based on ZnO/chitosan composite. *Talanta*, *69*, 686–690.

Wang, Z. L. (2004). Zinc oxide nanostructures: Growth, properties and applications. *Journal of Physics: Condensed Matter*, *16*, R829–R858.

Wei, A., Sun, X. W., Wang, J. X., Lei, Y., Cai, X. P., Li, C. M., et al. (2006). Enzymatic glucose biosensor based on ZnO nanorod array grown by hydrothermal decomposition. *Applied Physics Letters*, *89*, 123902.

Yamamoto, O. (2001). Influence of particle size on the antibacterial activity of zinc oxide. *International Journal of Inorganic Materials*, *3*, 643–646.

Yamamoto, O., Nakakoshi, K., Sasamoto, T., Nakagawa, H., & Miura, K. (2001). Adsorption and growth inhibition of bacteria on carbon materials containing zinc oxide. *Carbon*, *39*, 1643–1651.

Zhang, D. H., Wang, Q. P., & Xue, Z. Y. (2003). Photoluminescence of ZnO films excited with light of different wavelength. *Applied Surface Science*, *207*, 20–25.

Zhang, D. H., Xue, Z. Y., & Wang, Q. P. (2002). The mechanisms of blue emission from ZnO films deposited on glass substrate by R.F. magnetron sputtering. *Journal of Physics D: Applied Physics*, *35*, 2837–2840.

Zhang, Y., & Mu, J. (2007). Controllable synthesis of flower- and rod-like ZnO nanostructures by simply tuning the ratio of sodium hydroxide to zinc acetate. *Nanotechnology*, *18*, 075606.

Zhu, X., Yuri, I., Gan, X., Suzuki, I., & Li, G. (2007). Electrochemical study of the effect of nano-zinc oxide on microperoxidase and its application to more sensitive hydrogen peroxide biosensor preparation. *Biosensors and Bioelectronics*, *22*, 1600–1604.